Inorganic Chemistry

Article

pubs.acs.org/IC

Monodisperse Lanthanide Fluoride Nanocrystals: Synthesis and Luminescent Properties

Xingbo Li,[†] Shili Gai,[†] Chunxia Li,[‡] Dong Wang,[†] Na Niu,[†] Fei He,[†] and Piaoping Yang*[,†]

[†]Key Laboratory of Superlight Materials and Surface Technology, Ministry of Education, Harbin Engineering University, Harbin 150001, P. R. China

[‡]State Key Laboratory of Rare Earth Resource Utilization, Changchun Institute of Applied Chemistry, Chinese Academy of Sciences, Changchun 130021, P. R. China

Supporting Information

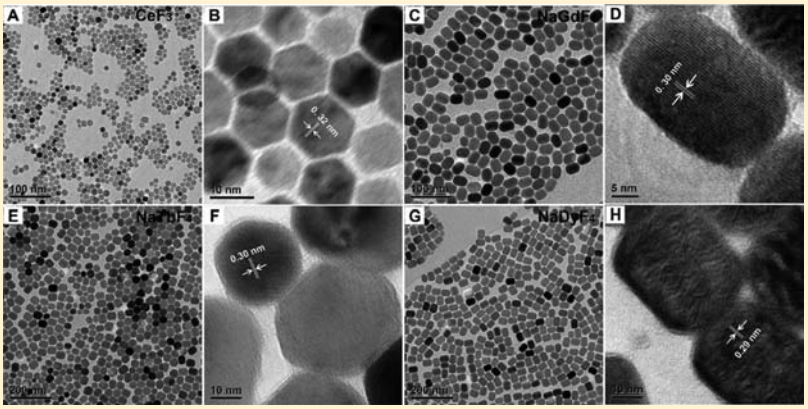

ABSTRACT: Three types of high-quality, monodisperse lanthanide fluoride colloidal nanocrystals (NCs) including LnF_3 (Ln = La−Pr), $NaLnF_4$ (Ln = Sm−Er), and $Na_5Ln_9F_{32}$ (Ln = Tm−Lu) with two crystal phases (hexagonal and cubic) and a rich variety of morphologies have been synthesized in high boiling organic solvents oleic acid and 1-octadecene, *via* a thermal decomposition pathway. The as-synthesized NCs were well characterized by X-ray diffraction (XRD), transmission electron microscopy (TEM), high resolution transmission electron microscopy (HRTEM), Fourier transform infrared spectroscopy (FT-IR), and photoluminescence (PL) spectra, respectively. It is found that the as-synthesized NCs consist of monodisperse nanoparticles with diverse shapes and narrow size distribution, which can easily disperse in nonpolar cyclohexane solvent. Additionally, a possible mechanism of NC nucleation and growth has been proposed. The results reveal that the formation of monodisperse NCs closely correlates with the inherent nature of lanthanide series from La to Lu. Under 980 nm NIR excitation, as-synthesized Yb^{3+}/Ln^{3+} (Ln = Er, Tm, Ho)-doped $NaGdF_4$ and $Na_5Lu_9F_{32}$ colloidal NCs show the respective characteristic up-conversion (UC) emissions of Er^{3+}, Tm^{3+}, and Ho^{3+}, which are promising for applications in biolabels, bioimaging, displays, and other optical technologies.

1. INTRODUCTION

In recent years, more and more attention has been focused on the nanomaterials, due to their unique size- and dimension-dependent electronic, optical, and magnetic properties and their potential applications as probes in various fields.[1] It is well-known that nanomaterials have interesting properties differing from their corresponding bulk materials. However, most nanomaterials often have a natural tendency toward aggregation, which always seems to be the main hindrance to their practical applications.[2] So the capability to control and manipulate the physical and chemical properties of materials as we desire is one of the challenging issues in chemistry and materials science.[3] Recently, the design and synthesis of inorganic NCs with well-defined morphologies and uniform size have stimulated great interest because the properties of the materials closely interrelate with geometrical factors such as shape, dimension, and size.[4] So far, many efforts have been devoted to explore efficient approaches for the fabrication of a variety of inorganic NCs to enhance their performance in current existing applications.[5]

Particularly, controlled synthesis of lanthanide fluoride NCs has attracted a lot of attention and has been a popular topic for the past decade[6] due to their potential use in optics, optoelectronics, microelectronics, and tribology.[7] In comparison with oxide materials, fluoride host materials provide some distinct advantages because of the low vibrational energies, and therefore the quenching of the excited states of the lanthanide ions will be minimal.[8] Furthermore, they exhibit adequate thermal and environmental stability and thus have been

Received: May 3, 2011
Published: March 12, 2012

extensively employed as ideal UC and down-conversion (DC) host matrixes for fluorescent rare earth ions.[9] Hitherto, many approaches including chemical vapor deposition (CVD),[10] sol–gel process,[11] microemulsion method,[12] nonhydrolytic route,[13] and hydro/solvothermal methods[14] have been extensively reported for the synthesis of lanthanide fluorides. However, for most reported methods until now, the synthesized fluorides have far from ideal uniformity and dispersibility, which dramatically limits their applications in biological fields. The widely employed hydrothermal/solvothermal process usually suffers from a low yield and long reaction time. Furthermore, the used toxic organometallic precursors or hazardous coordinating solvents have become matters of substantial environmental concern.[6f,g] Thus, the discovery and exploitation of an effective mass production and environmentally friendly approach to synthesize colloidal lanthanide fluoride NCs with well-defined shapes and good dispersibility should have great potential. Recently, Chen et al. reported the synthesis of $NaYF_4$ colloidal NCs with narrow size distribution *via* a two-step thermo-decomposition route.[6b] However, a systematic investigation of the general synthesis and properties of all of the other lanthanide fluoride colloidal NCs using a metal oleate thermal decomposition method has never been reported. Moreover, different from the extensive studies on the synthesis and applications of LnF_3 and $NaLnF_4$, little attention has been paid to the fabrication of other kinds of important lanthanide fluoride such as $Na_5Ln_9F_{32}$ colloidal NCs, which should also be promising materials based on their structural and optical properties.

Herein, we systematically report the general synthesis of three types of lanthanide fluoride colloidal NCs including LnF_3 (Ln = La–Pr), $NaLnF_4$ (Ln = Sm–Er), and $Na_5Ln_9F_{32}$ (Ln = Tm–Lu) with diverse shapes and narrow size distribution through a thermal decomposition method in a high boiling solvent. The NCs are well characterized by XRD, TEM, HRTEM, FT-IR, and photoluminescence (PL) spectra, respectively. A possible mechanism of the NCs' nucleation and growth is also proposed. The obtained NCs are well dispersed in nonploar cyclohexane solvent to form a stable and clear colloidal solution. The regular-shaped, monodisperse, and well-crystalline NCs exhibit a smooth surface and fewer crystal defects, which may endow them with potential applicability in biological and medical areas. This thermal decomposition method has proved to be one of the most efficient and powerful pathways to preparing novel nanostructures.[15]

2. EXPERIMENTAL SECTION

Reagents and Materials. Sodium fluoride (NaF) and HCl were obtained from Yili Chemical Corporation (Beijing, China). Lanthanide (Ln) oxides of SpecPure grade (La_2O_3, Pr_6O_{11}, Sm_2O_3, Eu_2O_3, Gd_2O_3, Tb_4O_7, Dy_2O_3, Ho_2O_3, Er_2O_3, Tm_2O_3, Yb_2O_3, Lu_2O_3, 99.99%), oleic acid, sodium oleate, and $Ce(NO_3)_3{\cdot}6H_2O$ were purchased from Sinopharm Chemical Reagent Co., Ltd. (Shanghai, China). 1-Octadecene (ODE) was purchased from Acros Organics. All of the chemical reagents were used as received without further purification. $LnCl_3$ was prepared by dissolving the corresponding lanthanide oxides in hydrochloric acid at an elevated temperature followed by evaporating the water under vacuum conditions.

Synthesis of Lanthanide Fluoride NCs. The synthesis of $Ln(oleate)_3$ complexes was performed *via* a modified procedure.[16] Typically, 1 mmol of $LnCl_3$, 30 mmol of sodium oleate, 15 mL of water, 20 mL of ethanol, and 35 mL of hexane were added to a 100 mL three-neck flask. The mixed solution was heated in a 70 °C water bath and kept at this temperature for 4 h under magnetic stirring. The obtained products were washed with deionized water three times in a funnel; the upper liquid was dried in an 80 °C water bath for several hours. In this way, the $Ln(oleate)_3$ complexes were obtained.

The synthesis of LnF_3 (La–Pr), $NaLnF_4$ (Sm–Er), and $Na_5Ln_9F_{32}$ (Tm–Lu) NCs was performed through a thermal decomposition synthetic approach. In a typical process for the synthesis of LaF_3 colloid NCs, 1 mmol of $La(oleate)_3$ and 5 mmol of NaF were first added to the mixed solvent of 15 mL of oleic acid and 15 mL of 1-octadecene simultaneously, then degassed under a nitrogen atmosphere for 30 min at 110 °C, and finally heated rapidly to 280 °C and kept at this temperature for 2.5 h under vigorous magnetic stirring in the presence of nitrogen. Subsequently, the mixture was allowed to cool to room temperature, and the NCs were precipitated by the addition of ethanol and isolated by centrifugation. The as-obtained NCs were washed several times with ethanol to remove the surplus oleic acid and other impurities. The final product was dispersed in nonpolar cyclohexane solvent to form a transparent colloidal solution. Other LnF_3 (Ln = Ce, Pr), $NaLnF_4$ (Ln = Sm–Er), and $Na_5Ln_9F_{32}$ (Ln = Tm–Lu) colloidal NCs were synthesized by a similar procedure except for using different lanthanide oleates.

Characterization. X-ray diffraction (XRD) was examined on a Rigaku-Dmax 2500 diffractometer using Cu Kα radiation (λ = 0.15405 nm). The morphologies and composition of the as-synthesized samples were characterized by transmission electron microscopy (TEM) and high-resolution transmission electron microscopey (HRTEM), performed on a FEI Tecnai G^2 S-Twin transmission electron microscope with a field emission gun operating at 200 kV. Samples for TEM measurements were prepared by evaporating a drop of the colloid onto a carbon-coated copper grid. The energy spectra were obtained by energy-dispersive X-ray spectrum (EDS, JEOL JXA-840) equipped on a scanning electron microscope (FESEM, S4800, Hitachi). Fourier-transform IR (FT-IR) spectra were measured on a Perkin-Elmer 580B IR spectrophotometer using the KBr pellet technique. The UC emission spectra were obtained using a 980 nm LD Module (K98D08M-30W, China) as the excitation source and were detected with an R955 (HAMAMATSU) detecting in the range of 400–900 nm. All of the measurements were performed at room temperature.

3. RESULTS AND DISCUSSION

Phase, Structure, and Morphologies. Figure 1 shows the XRD patterns of LnF_3 (Ln = La–Pr) NCs. It can be seen that

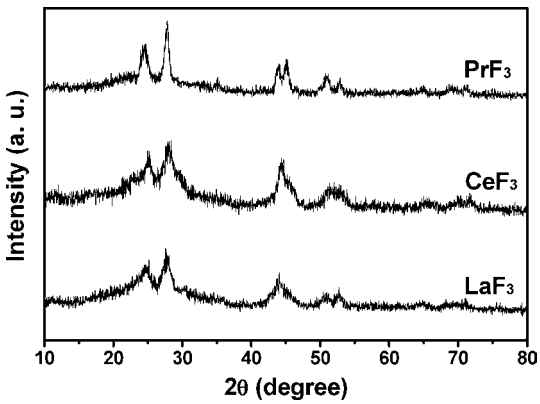

Figure 1. XRD patterns of as-synthesized LnF_3 (Ln = La–Pr) NCs with a hexagonal crystal structure.

all of the XRD patterns can be indexed to pure hexagonal LnF_3 (from La to Pr).[17] LaF_3 and PrF_3 NCs both belong to a $P\bar{3}c1$ (165) space group, while CeF_3 NCs have a $P6_3/mcm$ (193) space group. Lanthanide ions have gradually decreased ionic radii, and thus the physical and chemical properties should change accordingly.[18] The lattice constants (calculated from

dx.doi.org/10.1021/ic200925v | Inorg. Chem. 2012, 51, 3963–3971

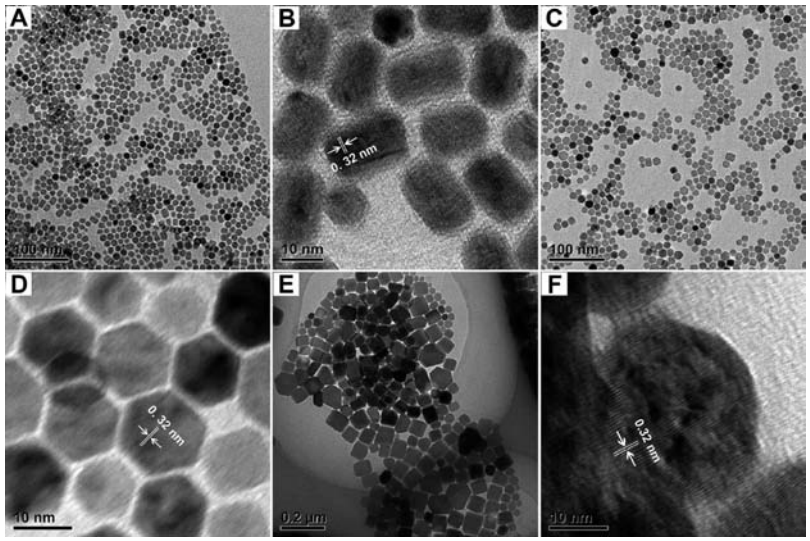

Figure 2. TEM and HRTEM images of LaF_3 (A, B), CeF_3 (C, D), and PrF_3 NCs (E, F).

MDI Jade 5.0) of LnF_3 in Table S1 (Supporting Information) are very close to their corresponding standard data, confirming the high crystallinity of the samples. In addition, the obvious broadening of the diffraction peaks reveals the nanosize nature of the as-synthesized NCs, which was used to calculate the average crystallite sizes according to the Scherrer formula $D = 0.89\lambda/(\beta \cos \theta)$, where D is the average grain size, λ is the X-ray wavelength (0.15405 nm), and θ and β are the diffraction angle and full-width at half-maximum (fwhm), respectively. As shown in Table S1, the average crystallite sizes for LaF_3, CeF_3 ,and PrF_3 NCs are calculated to be 12, 11, and 29 nm, respectively.

The morphologies and microstructures of LnF_3 NCs are characterized by TEM and HRTEM. Figure 2A, C, and E show the TEM images of LaF_3, CeF_3, and PrF_3 NCs, respectively. It can be seen that LaF_3 and CeF_3 NCs consist of uniform hexagonal nanoplates with good monodispersity, while PrF_3 NCs are composed of mixed hexagonal and quadrilateral nanoparticles with a much larger particle size. From Figure 2A, the average diameter of as-synthesized CeF_3 NCs (evaluated from 100 random particles) is also determined to be 12 nm, which is in good agreement with the XRD result (12 nm). In the corresponding HRTEM images of LaF_3 (Figure 2B), CeF_3 (Figure 2D), and PrF_3 NCs (Figure 3F), all three NCs are structurally uniform. The obvious lattice fringes indicate that NCs are highly crystalline. The distances of 0.32 nm between the adjacent lattice fringes agree well with the d_{111} spacing of hexagonal-phased LaF_3 (JCPDS No. 32-0483), CeF_3 (JCPDS No. 08-0045), and PrF_3 (JCPDS No. 46-1167), respectively.

With gradually decreased lanthanide ions (from Sm to Er), highly crystalline $NaLnF_4$ NCs indexed to pure hexagonal phases are obtained under the same synthetic conditions, which are shown in Figure 3. The diffraction peaks for all $NaLnF_4$ NCs are very similar in regard to shapes and intensities except for a slightly higher 2θ from Sm to Er, which should be caused by the increasing atomic number. Furthermore, much sharper and narrower peaks than those of LnF_3 are observed, implying larger crystal sizes and higher crystallinity. As shown in Table S1 (Supporting Information), the calculated lattice constants of $NaLnF_4$ NCs are also consistent with their corresponding standard data. Additionally, the calculated crystallite sizes summarized in Table S1 also suggest the nanosize nature of all of the samples.

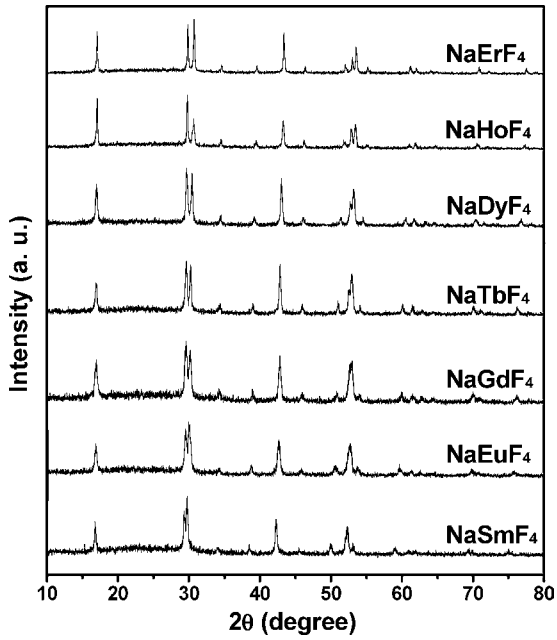

Figure 3. XRD patterns of as-synthesized $NaLnF_4$ (Ln = Sm−Er) NCs with a hexagonal crystal structure.

The morphologies and sizes change gradually with an increase in atomic number.[19] For $NaLnF_4$ (Sm to Er) NCs, the crystal phases of the products are identical (hexagonal), while their morphologies and sizes exhibit an apparent difference. As shown in Figure 4A, $NaSmF_4$ NCs are composed of well-dispersed cobblestone-like nanoparticles, $NaEuF_4$ NCs show two kinds of shapes (hexagonal and oval, Figure 4C), $NaGdF_4$ and $NaTbF_4$ NCs display uniform and monodispersed oval morphology (Figure 4E and G), $NaDyF_4$ NCs consist of rectangular nanoparticles (Figure 4I), $NaHoF_4$ NCs take the shape of well-dispersed square nanoparticles (Figure 4K), and $NaErF_4$ NCs exhibit square and hexagonal nanoplates (Figure 4M). The respective mean diameter is determined to be 32 nm for $NaSmF_4$, 26 nm for $NaEuF_4$, 27 nm for $NaGdF_4$, 36 nm for $NaTbF_4$, 38 nm for $NaDyF_4$, 64 nm for $NaHoF_4$, and 77 nm for $NaErF_4$, which are consistent with the average sizes calculated from XRD patterns in Table S1 (Supporting Information).

dx.doi.org/10.1021/ic200925v | Inorg. Chem. 2012, 51, 3963−3971

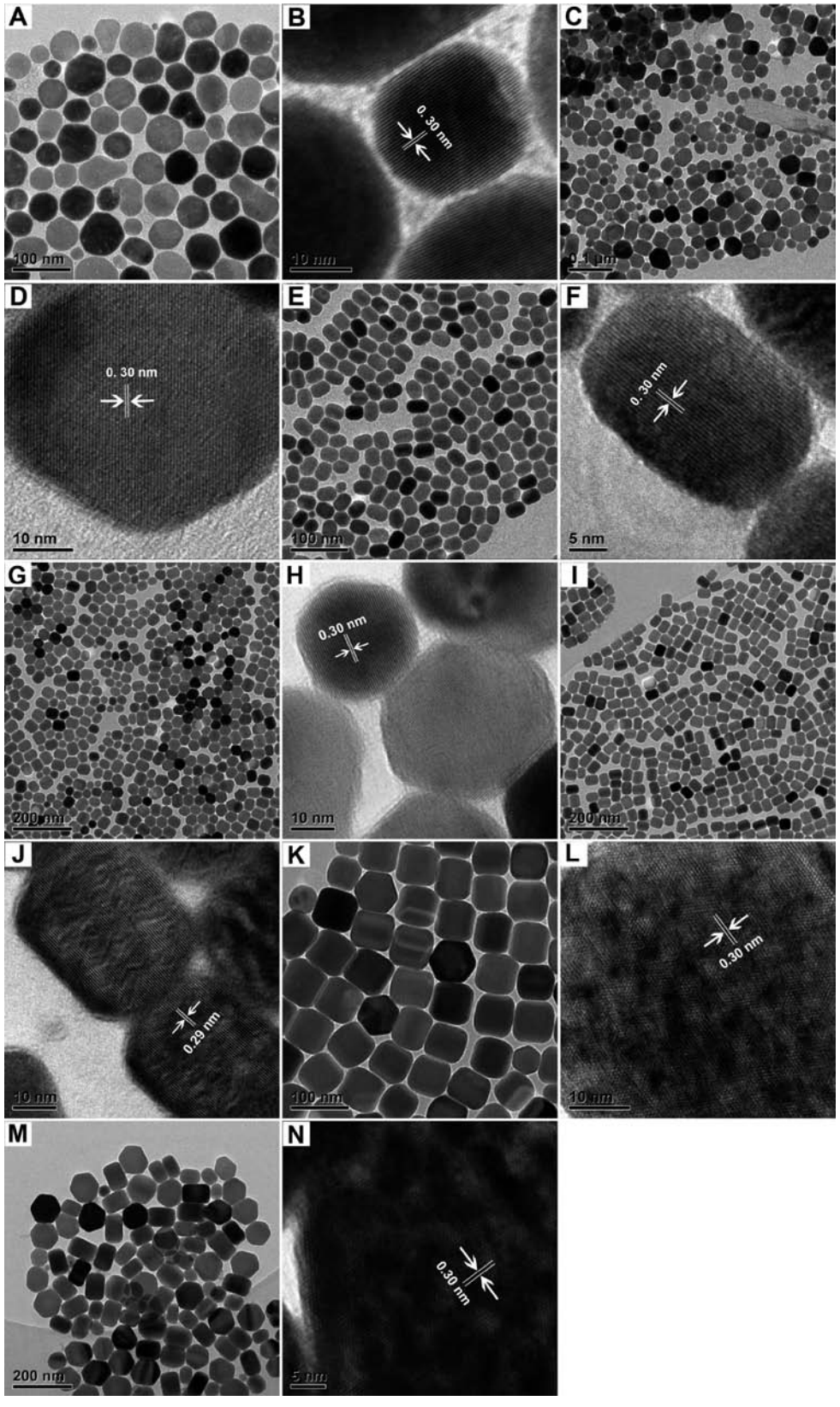

Figure 4. TEM and HRTEM images of $NaSmF_4$ (A, B), $NaEuF_4$ (C, D), $NaGdF_4$ (E, F), $NaTbF_4$ (G, H), $NaDyF_4$ (I, J), $NaHoF_4$ (K, L), and $NaErF_4$ NCs (M, N).

HRTEM image shows that these NCs have well-defined shapes and a highly crystalline nature. In Figure 4B, D, F, H, J, L, and N, for $NaLnF_4$ (from Sm to Er), the distance of the adjacent lattice fringes is determined to be about 0.30 nm, which corresponds well to the d_{111} spacing of hexagonal-phased $NaLnF_4$ (Ln = Sm−Er).

In our study, from Tm to Lu, the as-synthesized colloidal NCs display a completely different composition and phase. In

dx.doi.org/10.1021/ic200925v | *Inorg. Chem.* 2012, 51, 3963−3971

Figure 5, for the Tm-based sample, the XRD patterns are directly indexed to the standard card of cubic $Na_5Tm_9F_{32}$

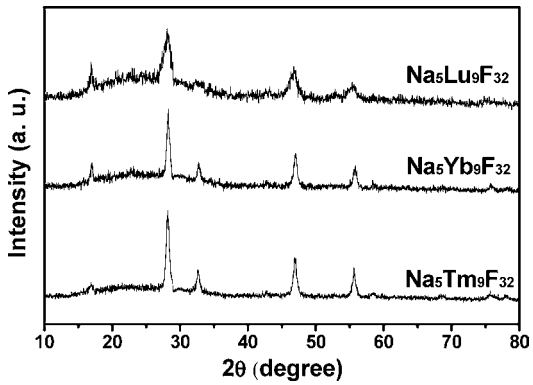

Figure 5. XRD patterns of as-synthesized $Na_5Ln_9F_{32}$ (Ln = Tm–Lu) NCs with a cubic crystal structure.

(JCPDS No. 27–0813) in the *Fm*3*m* space group. And the as-synthesized $Na_5Ln_9F_{32}$ (Ln = Yb, Lu) NCs can also be ascribed to the cubic crystal phase. The calculated lattice constants (Table S1, Supporting Information) are also very close to their corresponding standard data.

In Figure 6A, $Na_5Tm_9F_{32}$ NCs take the shape of an irregular hexagon with good monodispersity. In the corresponding

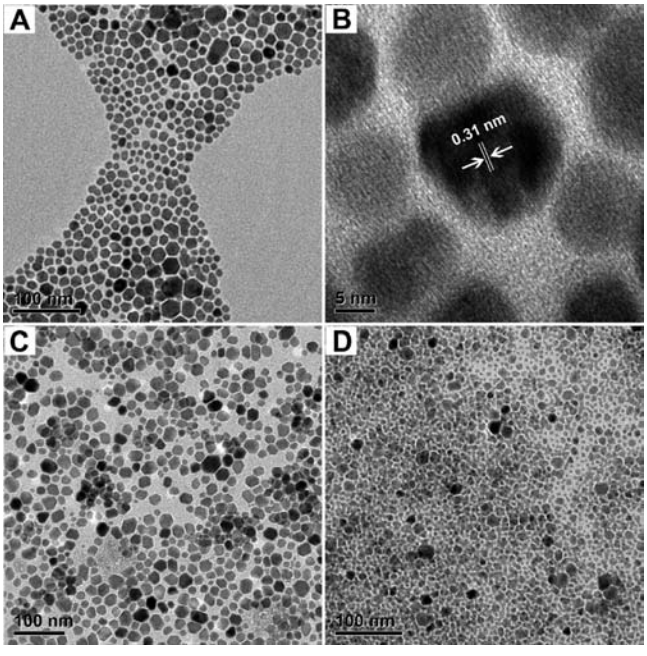

Figure 6. TEM (A) and HRTEM (B) of $Na_5Tm_9F_{32}$ and TEM images of $Na_5Yb_9F_{32}$ (C) and $Na_5Lu_9F_{32}$ (D).

HRTEM image (Figure 6B), the interplanar distance between the adjacent lattice fringes is determined to be 0.31 nm, corresponding well to the d_{111} space (0.315 nm) for cubic $Na_5Tm_9F_{32}$ (JCPDS No. 27-0813). In Figure 6C and D, $Na_5Yb_9F_{32}$ and $Na_5Lu_9F_{32}$ NCs exhibit a similar gravel morphology; their corresponding HRTEM image are not observed because adjacent lattice fringes are fuzzy. The respective average size is determined to be 22 nm for $Na_5Tm_9F_{32}$, 17 nm for $Na_5Yb_9F_{32}$, and 20 nm for $Na_5Lu_9F_{32}$, agreeing well with the values calculated from the XRD patterns.

Figure S1 (Supporting Information) shows the respective particle size distribution histograms of LnF_3 (Ln = La–Pr), $NaLnF_4$ (Ln = Sm–Er), and $Na_5Ln_9F_{32}$ (Ln = Tm–Lu) colloidal NCs, which were obtained by counting particle sizes on a minimum of 100 nanoparticles (the sizes of the elongated particles were determined by averaging of the long and the short axes). In the first group (La–Pr), it can be seen that the size distributions of LaF_3 and CeF_3 NCs are very similar, which are narrower than that of PrF_3 NCs. In the second group (Sm–Er), $NaGdF_4$, $NaTbF_4$, $NaDyF_4$, and $NaHoF_4$ NCs show apparently uniform size distributions, while other $NaLnF_4$ NCs exhibit relatively broader size distribution. As for $Na_5Ln_9F_{32}$ (Ln = Tm–Lu) NCs, broader size distributions are obtained.

The EDS spectra of all of the as-synthesized colloidal fluorides are shown in Figure 7. As shown, the EDS of LnF_3 (Ln = La, Ce, Pr) confirms the presence of elements F and La (Ce, Pr) in the product, and the obtained atomic ratio of F/Ln is well consistent with the theoretical atomic ratio (3:1). Similarly, EDS spectra of $NaLnF_4$ (Ln = Sm–Er) and $Na_5Ln_9F_{32}$ (Ln = Tm, Yb) present the elements F and Na and corresponding lanthanide ions in the products, and the atomic ratios of Na/Ln/F basically agree with the theoretically atomic ratios (4:1:1) in $NaLnF_4$ and (5:9:32) in $Na_5Ln_9F_{32}$.

FT-IR. FT-IR has been used to confirm the organic ligands on the NCs surface.[17] The oleic acid (OA) ligand plays an important role in the formation of monodisperse NCs in our system. It provides the obtained NCs with excellent stability and solubility in nonpolar solvents such as cyclohexane. The presence of the OA ligand can be shown in the FT-IR of LaF_3 NCs, as given in Figure 8. The very weak broad shoulder band at about 3440 cm^{-1} may be due to the O–H stretching vibration of the adsorbed water during the measurement process. The sharp absorption peak at 2924 cm^{-1} and the weak peak at 2960 cm^{-1} can be assigned to the symmetric (ν_s) and asymmetric (ν_{as}) stretching vibration of the $-CH_3$ group, and the peak at 2853 cm^{-1} is ascribed to the symmetric (ν_s) stretching of $-CH_2$ in the long alkyl chain of the oleic acid molecule.[20] The peak at 1701 cm^{-1} is assigned to the C=O stretching vibration, which is a characteristic peak for a metal–oleate complex. The sharp peaks at 1558 and 1461 cm^{-1} can be ascribed to the asymmetric (ν_{as}) and symmetric (ν_s) stretching vibrations of the deprotonated carboxylic group (CO_2^-), respectively. The peak at 723 cm^{-1} is assigned to the in-planar swing of $(CH_2)_n$ ($n > 4$).[21] On the basis of above analysis, it can be deduced that the oleic acid (OA) has successfully coated the NCs' surface, which endows the NCs with hydrophobic surfaces and leads to good dispersibility in nonpolar cyclohexane solvent.

Luminescence Properties. The UC luminescence of lanthanide-ion-doped fluorides has been extensively studied due to their potential applications in various fields, including lighting or display, IR detection, and biomedical imaging.[22] Lanthanide fluorides have been considered as an ideal host lattice for doping optically active lanthanide ions,[11] which exhibit different emission behaviors by tuning the doping components.[23] Figure 9 shows the up-conversion (UC) luminescence spectra of Yb^{3+}/Ln^{3+} (Ln = Er, Tm, Ho)-doped $NaGdF_4$ NCs under 980 nm laser excitation and their corresponding photographs in cyclohexane under 980 nm NIR irradiation. As shown, the $NaGdF_4$:Yb/Er, $NaGdF_4$:Yb/Tm, and $NaGdF_4$:Yb/Ho exhibit bright green, whitish blue, and

dx.doi.org/10.1021/ic200925v | Inorg. Chem. 2012, 51, 3963–3971

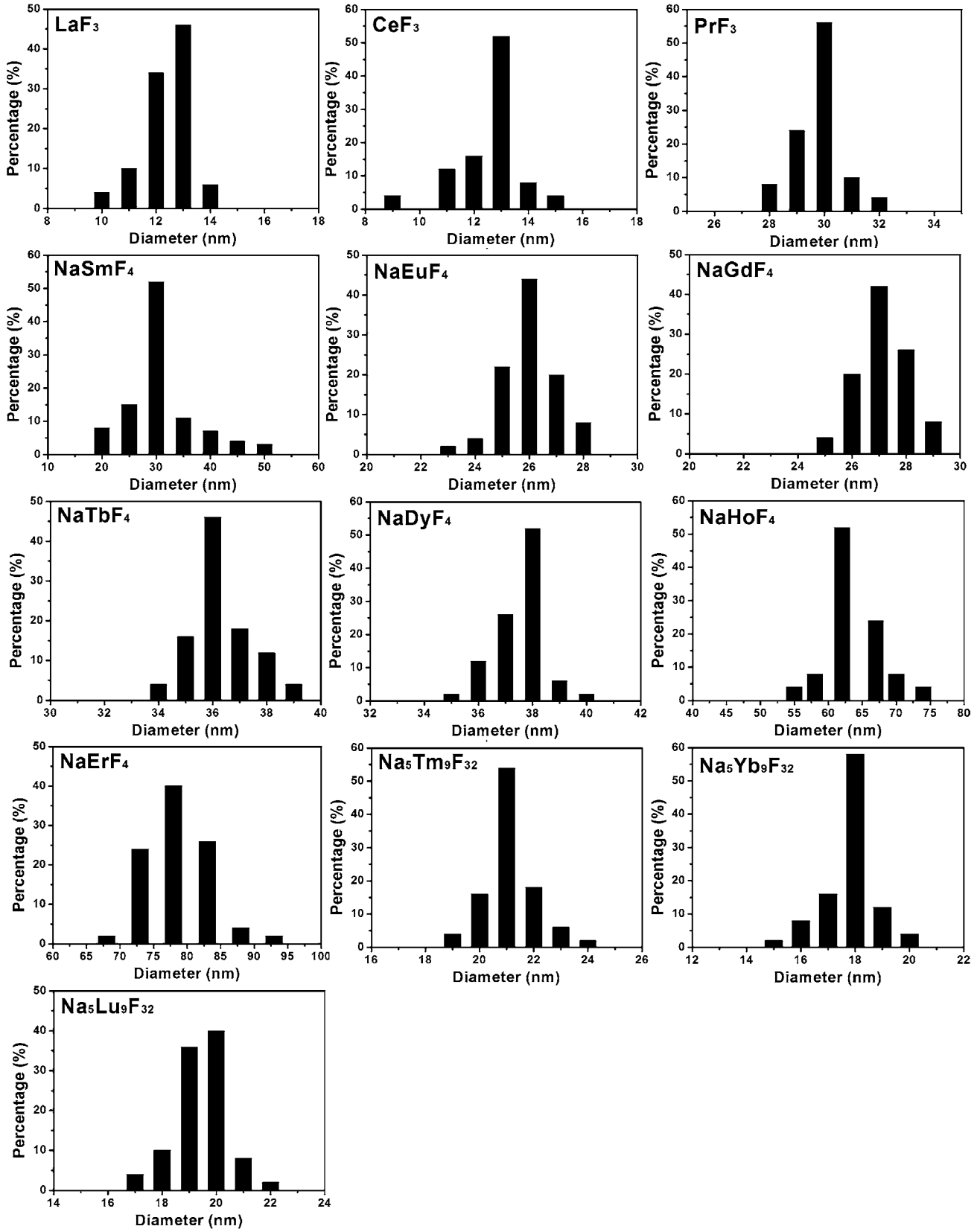

Figure 7. Particle size distribution histograms of LnF_3 (Ln = La−Pr), $NaLnF_4$ (Ln = Sm−Er), and $Na_5Ln_9F_{32}$ (Ln = Tm−Lu) NCs.

yellow-green emissions, respectively (insets in Figure 9). In the emission spectrum of $NaGdF_4$:Yb/Er NCs (Figure 9A), four emission peaks at 408, 521, 540, and 654 nm can be assigned to the $^2H_{9/2} \rightarrow {}^4I_{15/2}$, $^2H_{11/2} \rightarrow {}^4I_{15/2}$, $^4S_{3/2} \rightarrow {}^4I_{15/2}$, and $^4F_{9/2} \rightarrow {}^4I_{15/2}$ transitions of Er^{3+}, respectively.[24,25] The dominated green emission centered at 510−560 nm results in the green color of the NCs. For $NaGdF_4$:Yb/Tm NCs (Figure 9B), the intense blue emissions at 450 and 475 nm correspond to the $^1D_2 \rightarrow {}^3F_4$

dx.doi.org/10.1021/ic200925v | Inorg. Chem. 2012, 51, 3963−3971

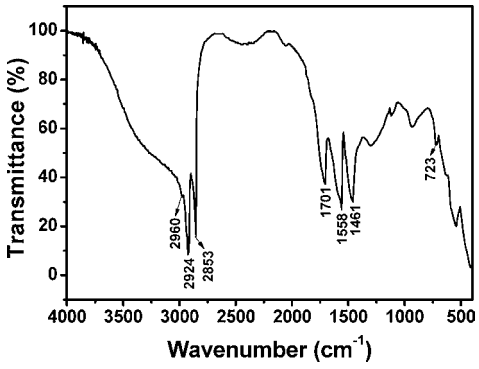

Figure 8. FT-IR spectrum of representative LaF_3 NCs.

and $^1G_4 \rightarrow {}^3H_6$ transitions; the weak red emission peaks at 645 and 698 nm can be attributed to the transitions of $^1G_4 \rightarrow {}^3F_4$ and $^3F_3 \rightarrow {}^3H_6$, respectively.[26] In Figure 9C, for $NaGdF_4$:Yb/Ho, the strong green emission at 541 nm can be associated with the $^5F_4$ and $^5S_2$ levels to the $^5I_8$ ground state. The relatively weak blue emission at 486 nm and the red emission at 645 nm may originate from $^5F_3 \rightarrow {}^5I_8$ and $^5F_5 \rightarrow {}^5I_8$ transitions.[27]

The synthesis of $Na_5Lu_9F_{32}$ colloidal NCs, especially the UC luminescent properties of Yb/Er (Tm, Ho)-codoped $Na_5Lu_9F_{32}$ NCs, has never been reported. Here, 18% Yb^{3+} and 2% Er^{3+} (Tm^{3+}, Ho^{3+}) were selected as the doping ions to study the luminescent properties. As shown in Figure 10, the

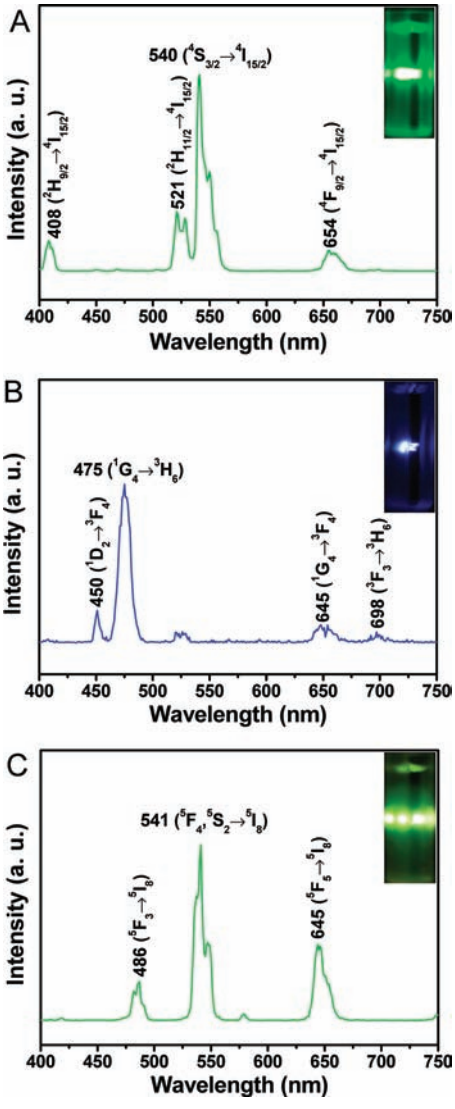

Figure 9. UC emission spectra of $NaGdF_4$:Yb/Er (A), $NaGdF_4$:Yb/Tm (B), and $NaYF_4$:Yb/Ho (C) under 980 nm laser diode excitation. The insets are their corresponding photographs in cyclohexane solution under 980 nm NIR irradiation.

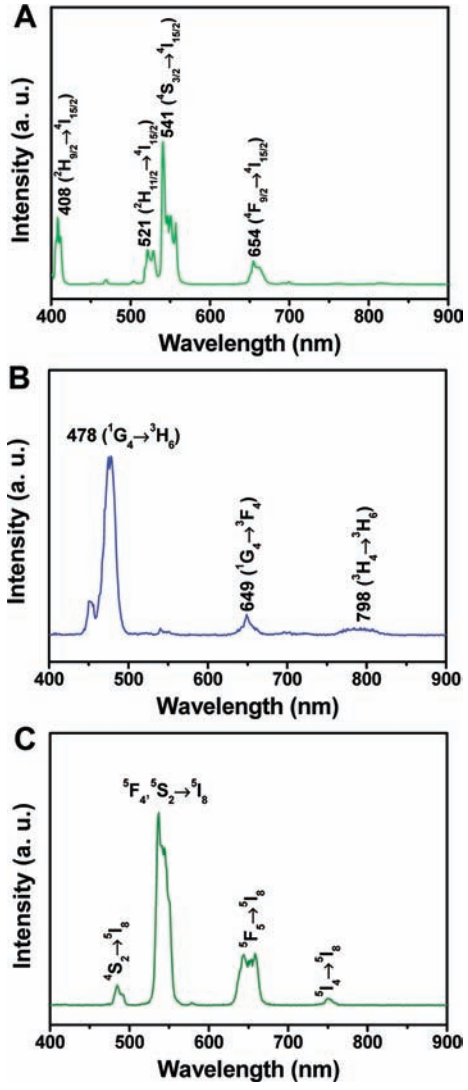

Figure 10. NIR-to-visible UC emission spectra of $Na_5Lu_9F_{32}$:Yb/Er (A), $Na_5Lu_9F_{32}$:Yb/Tm (B), and $Na_5Lu_9F_{32}$:Yb/Ho (C).

$Na_5Lu_9F_{32}$:Yb/Er, $Na_5Lu_9F_{32}$:Yb/Tm, and $Na_5Lu_9F_{32}$:Yb/Ho NCs show very similar emission peak positions to those of $NaGdF_4$:Ln NCs. However, the relative emission intensities of red emission (654 nm), green emission (521 nm, 540 nm), and blue emission (478 nm) change obviously, which should exhibit different emission colors.

Possible Formation and Growth Mechanism. In general, a typical system for the synthesis of colloidal NCs is composed of three parts: precursors, organic surfactants, and solvents.[28] As demonstrated by Steigerwald, the first key step in the generation of colloidal NCs is the identification of suitable precursor molecules.[29] The employed precursors are relatively simple molecules with "leaving groups" that readily depart to

dx.doi.org/10.1021/ic200925v | Inorg. Chem. 2012, 51, 3963–3971

leave behind the desired reactive species successfully, which allows for nucleation to be separated in time from the growth step to obtain NCs with relatively narrow size distribution. The precursors were obtained by an ion exchange process between lanthanide chloride and sodium oleate, leading to the formation of lanthanide oleate complexes through a strong coordination interaction. In our cases, the precursors of lanthanide oleate may decompose rapidly above 280 °C in organic solvents, which can allow for the occurrence of nucleation as a separated step. According to the proposed reaction mechanism, the formation of lanthanide oleate complexes seems to play a key role in the monodisperse NCs.

In this system, a liquid−solid two-phase approach was used to synthesize monodisperse NCs. Lanthanide oleate complexes were dissolved in the organic solvent as the liquid phase. And NaF dispersed in the same organic solvent was used as the solid phase due to the insolubility in 1-octadecene.[6b] The formation of the NCs involves two steps: nucleation of an initial seed, and subsequent growth. In the nucleation step, the precursors of lanthanide oleate complexes decompose at a high temperature (280 °C) to form monomers. Ln^{3+} is then free from the lanthanide oleate complexes; Na^+ and F^- ions are dispersed in organic solvent at the same time. Oleic acid capped Ln^{3+} quickly reacts with F^- and Na^+ to form nuclei of as-obtained lanthanide fluorides. It is possible that oleic acid molecules modulate the growth rate along certain directions, which results in a variety of NCs with different shapes. The selective adsorption of oleic acid onto crystal facets induces the morphology change of lanthanide fluoride NCs, which can be explained by the selective-adsorption model.[30] According to this model, a surfactant is required for anisotropic growth, which provides selective adsorption of surfactants at different crystallographic faces of the growing crystals, leading to different crystallographic growth along these planes. The preferred adsorption of oleic acid on the [0001] surfaces of the hexagonal lanthanide fluorides makes the NCs grow more anisotropically along the [10$\bar{1}$0] direction, while the preferred adsorption of oleic acid on the [001] surfaces makes the NCs grow more anisotropically along the [100] direction for cubic lanthanide fluorides. A proper schematic illustration for the growth of lanthanide fluoride NCs is provided in Scheme 1. Furthermore, the controlled synthesis of fluoride NCs in the present work can be simply explained from the point of view of system-free energy.[31] For group I in OA/ODE, uniform LnF_3 (Ln = La, Ce, and Pr) hexagonal nanoplates are directly formed using $Ln(oleate)_3$ and NaF as the precursors because $NaLnF_4$ is not as stable as LnF_3. For group II, β-$NaLnF_4$ (Ln = Sm to Er) NCs are formed directly in OA/ODE. As the energy barrier was considered to be relatively low, the growth of β-$NaLnF_4$ should be so fast that only irregular nanoparticles are achieved. For group III, the energy barrier to the formation of β-$NaLnF_4$ is so high that β-$NaLnF_4$ is not stable in OA/ODE. Thus, $Na_5Ln_9F_{32}$ (Ln = Tm to Lu) with low free energy can be obtained. More ions (Ln^{3+}, Na^+ and F^-) taking part in the nucleation and growth of $Na_5Ln_9F_{32}$ may result in the irregular hexagons of the final product.

Scheme 1. Schematic Illustration of the Mode for the Growth of LnF_3 (Ln = La−Pr), $NaLnF_4$ (Ln = Sm−Er), and $Na_5Ln_9F_{32}$ (Ln = Tm−Lu) NCs with Different Morphologies

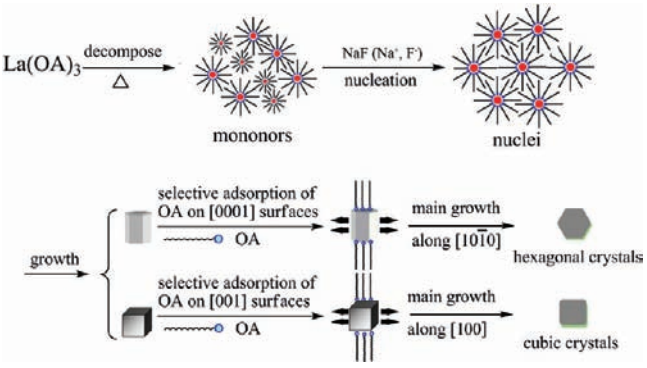

4. CONCLUSIONS

In summary, we presented a facile route to synthesize high-quality lanthanide fluoride including LnF_3 (Ln = La−Pr), $NaLnF_4$ (Ln = Sm−Er), $Na_5Ln_9F_{32}$ (Ln = Tm−Lu) colloidal NCs based on the thermal decomposition of corresponding lanthanide oleate precursors in organic solvent (oleic acid and 1-octadecene), where oleic acid used as a surfactant played a crucial role in the formation process of the NCs. All of the obtained NCs have good monodispersity and good solubility in cyclohexane to form stable and clear colloidal solutions. Furthermore, room-temperature luminescent studies have revealed that as-obtained Yb^{3+}/Ln^{3+} (Ln = Er, Tm, Ho)-doped $NaGdF_4$ and $Na_5Lu_9F_{32}$ NCs can exhibit intensive up-conversion luminescence under 980 nm excitation, which is promising for applications in multiple biolabels, staining, and displays. These results not only enrich the contents of lanthanide fluoride chemistry but also provide fundamental insight into the crystal growth and formation mechanism of nanosized materials.

■ ASSOCIATED CONTENT

Ⓢ Supporting Information

Calculated lattice constants, crystal phases, morphologies, and average crystallite sizes and particle size distribution histograms of LnF_3. This material is available free of charge via the Internet at http://pubs.acs.org.

■ AUTHOR INFORMATION

Corresponding Author

*E-mail: yangpiaoping@hrbeu.edu.cn.

Notes

The authors declare no competing financial interest.

■ ACKNOWLEDGMENTS

Financial support from the National High Technology Research Program of China (2011AA03A407), National Basic Research Program of China (2010CB327704) Research Fund for the Doctoral Program of Higher Education of China (20112304110021), and the Fundamental Research Funds for the Central Universities of China (HEUCF201210009) are acknowledged.

■ REFERENCES

(1) (a) Chan, E. M.; Xu, C. X.; Mao, A. W.; Han, G.; Owen, J. S.; Cohen, B. E.; Milliron, D. J. *Nano Lett.* **2010**, *10*, 1874. (b) Park, Y. I.; Kim, J. H.; Lee, K. T.; Jeon, K. S.; Bin Na, H.; Yu, J. H.; Kim, H. M.; Lee, N.; Choi, S. H.; Baik, S. I.; Kim, H.; Park, S. P.; Park, B. J.; Kim, Y. W.; Lee, S. H.; Yoon, S. Y.; Song, I. C.; Moon, W. K.; Suh, Y. D.; Hyeon, T. *Adv. Mater.* **2009**, *21*, 4467. (c) Iijima, S. *Nature* **1991**, *354*, 56. (d) Wang, X.; Zhuang, J.; Peng, Q.; Li, Y. D. *Adv. Mater.* **2006**, *18*, 2031. (e) Murray, C. B.; Norris, D. J.; Bawendi, M. G. *J. Am. Chem.*

Soc. **1993**, *115*, 8706. (f) Wang, X.; Zhuang, J.; Peng, Q.; Li, Y. D. *Nature* **2005**, *437*, 121. (g) Yu, T.; Joo, J.; Park, Y. I.; Hyeon, T. *J. Am. Chem. Soc.* **2006**, *128*, 1786.
(2) Vetrone, F.; Capobianco, J. A. *Int. J. Nanotechnol.* **2008**, *5*, 1306.
(3) Milliron, D. J.; Hughes, S. M.; Cui, Y.; Manna, L.; Li, J. B.; Wang, L. W.; Alivisatos, A. P. *Nature* **2004**, *430*, 190.
(4) (a) Alivisatos, A. P. *Science* **1996**, *271*, 933. (b) Jun, Y. W.; Choi, J. S.; Cheon, J. *Angew. Chem., Int. Ed.* **2006**, *45*, 3414. (c) Wang, Z. L.; Hao, J. H.; Chan, H. L. W. *J. Mater. Chem.* **2010**, *20*, 3178. (d) Chan, T. S.; Liu, R. S.; Baginskiy, I. *Chem. Mater.* **2008**, *20*, 1215.
(5) (a) Li, C. X.; Quan, Z. W.; Yang, P. P.; Yang, J.; Lian, H. Z.; Lin, J. *J. Mater. Chem.* **2008**, *18*, 1353. (b) Sun, X.; Zhang, Y. W.; Du, Y. P.; Yan, Z. G.; Si, R.; You, L. P.; Yan, C. H. *Chem.—Eur. J.* **2007**, *13*, 2320. (c) Kang, C. C.; Liu, R. S.; Chang, J. C.; Lee, B. J. *Chem. Mater.* **2003**, *15*, 3966. (d) Zhou, S. F.; Jiang, N.; Wu, B. T.; Hao, J. H.; Qiu, J. R. *Adv. Funct. Mater.* **2009**, *19*, 2081. (e) Chen, L.; Chen, K. J.; Lin, C. C.; Chu, C.; Hu, S. F.; Lee, M. H.; Liu, R. S. *J. Comb. Chem.* **2010**, *12*, 587. (f) Chen, H. M.; Peng, H. C.; Liu, R. S.; Asakura, K.; Lee, C. L.; Lee, J. F.; Hu, S. F. *J. Phys. Chem. B* **2005**, *109*, 19553. (g) Wang, H.; Duan, C.-K.; Tanner, P. A. *J. Phys. Chem. C* **2008**, *112*, 16651. (h) Wang, J. W.; Hao, J. H.; Tanner, P. A. *Opt. Lett.* **2910**, *35*, 3922.
(6) (a) Wang, F.; Han, Y.; Lim, C. S.; Lu, Y.; Wang, J.; Xu, J.; Chen, H.; Zhang, C.; Hong, M.; Liu, X. *Nature* **2010**, *463*, 1061. (b) Wei, Y; Lu, F. Q.; Zhang, X. R.; Chen, D. P. *Chem. Mater.* **2006**, *18*, 5733. (c) Zhang, Y. W.; Sun, X.; Si, R.; You, L. P.; Yan, C. H. *J. Am. Chem. Soc.* **2005**, *127*, 3260. (d) Duan, C.-K.; Tanner, P. A.; Babin, V.; Meijerink, A. *J. Phys. Chem. C* **2009**, *113*, 12580. (e) Wang, F.; Liu, X. G. *Chem. Soc. Rev.* **2009**, *38*, 976. (f) Mai, H. X.; Zhang, Y. W.; Si, R.; Yan, Z. G.; Sun, L. D.; You, L. P.; Yan, C. H. *J. Am. Chem. Soc.* **2006**, *128*, 6426. (g) Yi, G. S.; Chow, G. M. *Chem. Mater.* **2007**, *19*, 341.
(7) (a) Hebbink, G. A.; Stouwdam, J. W.; Reinhoudt, D. N.; van Veggel, F. *Adv. Mater.* **2002**, *14*, 1147. (b) Stouwdam, J. W.; van Veggel, F. *Nano Lett.* **2002**, *2*, 733. (c) Wang, X.; Li, Y. D. *Chem. Commun.* **2007**, 2901. (d) Zimer, H.; Albers, K.; Wittrock, U. *Opt. Lett.* **2004**, *29*, 2761. (e) Terada, Y.; Shimamura, K.; Kochurikhin, V. V.; Barashov, L. V.; Ivanov, M. A.; Fukuda, T. *J. Cryst. Growth* **1996**, *167*, 369.
(8) Bender, C. M.; Burlitch, J. M.; Barber, D.; Pollock, C. *Chem. Mater.* **2000**, *12*, 1969.
(9) (a) Zhang, S. Z.; Sun, L. D.; Tian, H.; Liu, Y.; Wang, J. F.; Yan, C. H. *Chem. Commun.* **2009**, *18*, 2547. (b) Xu, Z. H.; Li, C. X.; Yang, P. P.; Zhang, C. M.; Huang, S. S.; Lin, J. *Cryst. Growth Des.* **2009**, *9*, 4752. (c) Zeng, J. H.; Su, J.; Li, Z. H.; Yan, R. X.; Li, Y. D. *Adv. Mater.* **2005**, *17*, 2119. (d) Liang, X.; Wang, X.; Zhuang, J.; Chen, Y. T.; Wang, D. S.; Li, Y. D. *Adv. Funct. Mater.* **2006**, *16*, 1805. (e) Zhang, F.; Wan, Y.; Yu, T.; Zhang, F. Q.; Shi, Y. F.; Xie, S. H.; Li, Y. G.; Xu, L.; Tu, B.; Zhao, D. Y. *Angew. Chem., Int. Ed.* **2007**, *46*, 7976. (f) Heer, S.; Kompe, K.; Gudel, H. U.; Haase, M. *Adv. Mater.* **2004**, *16*, 2102. (g) Wang, J. A.; Wang, F.; Xu, J.; Wang, Y.; Liu, Y. S.; Chen, X. Y.; Chen, H. Y.; Liu, X. G. *C. R. Chim.* **2010**, *13*, 731.
(10) Meng, Q. G.; Witte, R. J.; May, P. S.; Berry, M. T. *Chem. Mater.* **2009**, *21*, 5801.
(11) Sudarsan, V.; Sivakumar, S.; van Veggel, F.; Raudsepp, M. *Chem. Mater.* **2005**, *17*, 4736.
(12) Aubert, T.; Grasset, F.; Mornet, S.; Duguet, E.; Cador, O.; Cordier, S.; Molard, Y.; Demange, V.; Mortier, M.; Haneda, H. *J. Colloid Interface Sci.* **2010**, *341*, 201.
(13) Mutin, P. H.; Vioux, A. *Chem. Mater.* **2009**, *21*, 582.
(14) Zhang, L. X.; Sun, Y. X.; Jiu, H. F.; Han, X. W.; Fan, T.; Liu, G. D. *Micro. Nano Lett.* **2011**, *6*, 22.
(15) (a) Qian, H. S.; Guo, H. C.; Ho, P. C. L.; Mahendran, R.; Zhang, Y. *Small* **2009**, *5*, 2285. (b) Liang, J. H.; Peng, C.; Wang, X.; Zheng, X.; Wang, R. J.; Qiu, X. P. P; Nan, C. W.; Li, Y. D. *Inorg. Chem.* **2005**, *44*, 9405.
(16) Park, J.; An, K.; Hwang, Y.; Park, J. G.; Noh, H. J.; Kim, J. Y.; Park, J. H.; Hwang, N. M.; Hyeon, T. *Nat. Mater.* **2004**, *3*, 894.
(17) Quan, Z. W.; Yang, P. P.; Li, C. X.; Yang, J.; Yang, D. M.; Jin, Y.; Lian, H. Z.; Li, H. Y.; Lin, J. *J. Phys.Chem. C* **2009**, *113*, 4018.
(18) Li, C. X.; Liu, X. M.; Yang, P. P.; Zhang, C. M.; Lian, H. Z.; Lin, J. *J. Phys. Chem. C* **2008**, *112*, 15602.
(19) Li, C. X.; Yang, J.; Yang, P. P.; Lian, H. Z.; Lin, J. *Chem. Mater.* **2008**, *20*, 4317.
(20) (a) Tao, Y. T. *J. Am. Chem. Soc.* **1993**, *115*, 4350. (b) Allara, D. L.; Nuzzo, R. G. *Langmuir* **1985**, *1*, 45. (c) Schlotter, N. E.; Porter, M. D.; Bright, T. B.; Allara, D. L. *Chem. Phys. Lett.* **1986**, *132*, 93. (d) Chau, L. K.; Porter, M. D. *Chem. Phys. Lett.* **1990**, *167*, 198.
(21) Zhang, X. M.; Quan, Z. W.; Yang, J.; Yang, P. P.; Lian, H. Z.; Lin, J. *Nanotechnology* **2008**, *19*, 075603.
(22) (a) Schafer, H.; Ptacek, P.; Kompe, K.; Haase, M. *Chem. Mater.* **2007**, *19*, 1396. (b) Aebischer, A.; Heer, S.; Biner, D.; Kramer, K.; Haase, M.; Gudel, H. U. *Chem. Phys. Lett.* **2005**, *407*, 124. (c) Lehmann, O.; Meyssamy, H.; Kompe, K.; Schnablegger, H.; Haase, M. *J. Phys. Chem. B* **2003**, *107*, 7449.
(23) Diamente, P. R.; Burke, R. D.; van Veggel, F. *Langmuir* **2006**, *22*, 1782.
(24) Yi, G. S.; Lu, H. C.; Zhao, S. Y.; Yue, G.; Yang, W. J.; Chen, D. P.; Guo, L. H. *Nano Lett.* **2004**, *4*, 2191.
(25) (a) Suyver, J. F.; Grimm, J.; van Veen, M. K.; Biner, D.; Kramer, K. W.; Gudel, H. U. *J. Lumin.* **2006**, *117*, 1. (b) Lu, H. C.; Yi, G. S.; Zhao, S. Y.; Chen, D. P.; Guo, L. H.; Cheng, J. *J. Mater. Chem.* **2004**, *14*, 1336.
(26) (a) Li, Z. Q.; Zhang, Y. *Nanotechnology* **2008**, *19*, 345606. (b) Suyver, J. F.; Aebischer, A.; Biner, D.; Gerner, P.; Grimm, J.; Heer, S.; Kramer, K. W.; Reinhard, C.; GMdel, H. U. *Opt. Mater.* **2005**, *27*, 1111.
(27) Yang, L. W.; Han, H. L.; Zhang, Y. Y.; Zhong, J. X. *J. Phys. Chem. C* **2009**, *113*, 18995.
(28) Yin, Y.; Alivisatos, A. P. *Nature* **2005**, *437*, 664.
(29) Steigerwald, M. L. *Polyhedron* **1994**, *13*, 1245.
(30) (a) Manna, L.; Scher, E. C.; Alivisatos, A. P. *J. Am. Chem. Soc.* **2000**, *122*, 12700. (b) Kumar, S.; Nann, T. *Small* **2006**, *2*, 316.
(31) (a) Jun, Y. W.; Lee, J. H.; Choi, J. S.; Cheon, J. *J. Phys. Chem. B* **2005**, *109*, 14795. (b) Chen, Y. F.; Kim, M.; Lian, G. D.; Johnson, M. B.; Peng, X. G. *J. Am. Chem. Soc.* **2005**, *127*, 13331.